1-1-2017

Biocompatible Copper Oxide Nanoparticle Composites from Cellulose and Chitosan: Facile Synthesis, Unique Structure, and Antimicrobial Activity

Chieu D. Tran
Marquette University, chieu.tran@marquette.edu

James Makuvaza

Erik Munson
Marquette University, erik.munson@marquette.edu

Brian Bennett
Marquette University, brian.bennett@marquette.edu

Accepted version. *ACS Applied Materials & Interfaces*, Vol. 9, No. 49 (2017): 42503-42515. DOI.

Biocompatible Copper Oxide Nanoparticle Composites from Cellulose and Chitosan: Facile Synthesis, Unique Structure, and Antimicrobial Activity

Chieu D. Tran

Department of Chemistry, Marquette University, Milwaukee, WI

James Makuvaza

Department of Chemistry, Marquette University, Milwaukee, WI

Erik Munson

Department of Chemistry, Marquette University, Milwaukee, WI

Brian Bennett

Department of Physics, Marquette University, Milwaukee, WI

Abstract

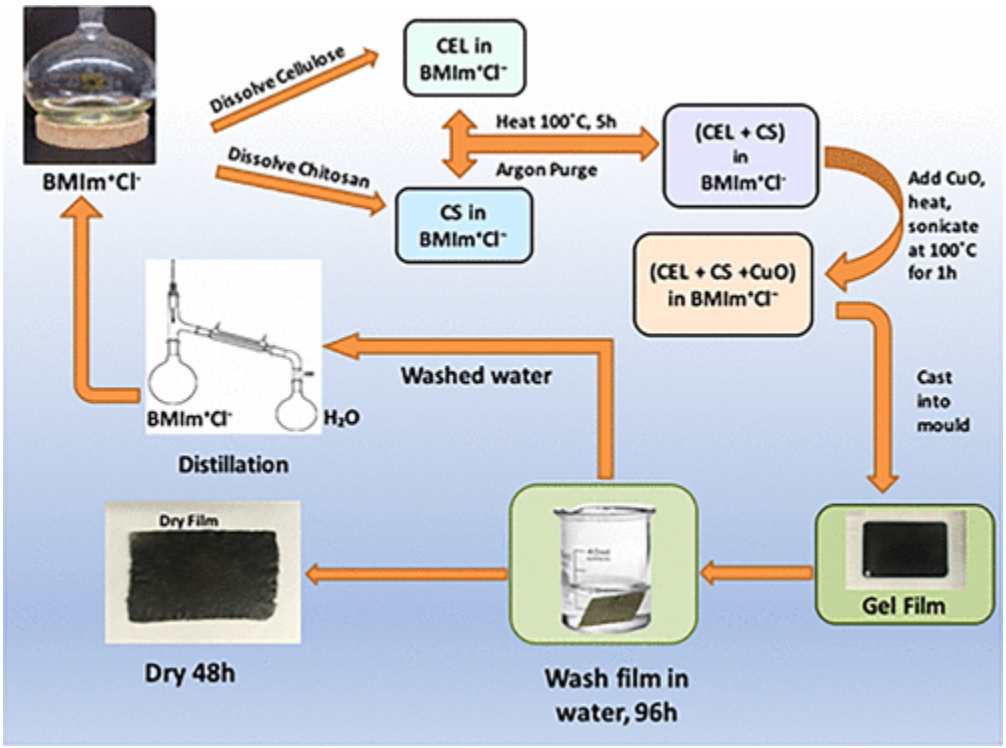

Copper in various forms has been known to have bactericidal activity. Challenges to its application include preventing mobilization of the copper, to both extend activity and avoid toxicity, and bioincompatibility of many candidate substrates for copper immobilization. Using a simple ionic liquid, butylmethylimmidazolium chloride as the solvent, we developed a facile and green method to synthesize biocompatible composites containing copper oxide nanoparticles (CuONPs) from cellulose (CEL) and chitosan (CS) or CEL and keratin (KER). Spectroscopy and imaging results indicate that CEL, CS, and KER remained chemically intact and were homogeneously distributed in the composites with CuONPs with size of 22 ± 1 nm. Electron paramagnetic resonance (EPR) suggests that some 25% of the EPR-detectable Cu(II) is present as a monomeric species, chemically anchored to the substrate by two or more nitrogen atoms, and, further, adopts a unique spatially oriented conformation when incorporated into the [CEL + CS] composite but not in the [CEL + KER] composite. The remaining 75% of EPR-detectable Cu(II) exhibited extensive spin–spin interactions, consistent with Cu(II) aggregates and Cu(II) on the surface of CuONPs. At higher levels of added copper (>59 nmol/mg), the additional copper was EPR-silent, suggesting an additional phase in larger CuONPs, in which $S > 0$ spin states are either thermally inaccessible or very fast-relaxing. These data suggest that Cu(II) initially binds substrate via nitrogen atoms, from which CuONPs develop through aggregation of copper. The composites exhibited excellent antimicrobial activity against a wide range of bacteria and fungi, including methicillin-resistant *Staphylococcus aureus*; vancomycin-resistant *Enterococcus*; and highly resistant *Escherichia coli*, *Streptococcus agalactiae*, *Pseudomonas aeruginosa*, *Stenotrophomonas maltophilia*, and *Candida albicans*. Expectedly, the antibacterial activity was found to be correlated with the CuONPs content in the composites. More importantly, at CuONP concentration of 35 nmol/mg or lower, bactericidal activity of the composite was complemented by its biocompatibility with human fibroblasts.

Keywords:
antibacteria; biocompatible; cellulose; chitosan; copper oxide nanoparticles; EPR; fungi; ionic liquid

Introduction

Copper ions, alone or in copper complexes, have been employed for centuries to disinfect solids, liquids, and human tissue.[1-8] For example, copper oxide nanoparticles (CuONPs) inhibit pathogenic bacteria, such as *Klebsiella pneumoniae*, *Shigella dysenteriae*, *Staphylococcus aureus*, *Salmonella typhimurium*, and *Escherichia coli*, which are responsible for delayed wound healing in humans. Copper ions have also been used as antiviral agents to treat herpes simplex, influenza, MS2 *coliphage*, and hepatitis A viruses.[1-8] Furthermore, when compared to silver and gold nanoparticles, CuONPs demonstrate additional advantages of being inexpensive and chemically stable.

The size, morphology, and stability of nanoparticles (NPs) strongly affect their antimicrobial activity.[9-13] Colloidal NPs are known to undergo aggregation and coagulation in solution, leading to changes in their size, morphology, and antibacterial properties. An effective and reliable method to incorporate CuONPs into a supporting material to prevent coagulation and aggregation to maintain antimicrobial activity is, therefore, needed. CuONPs have been encapsulated by various polymers and/or copolymers (e.g., methacrylic acid copolymer beads), with retention of antimicrobial activity.[14] However, each of these systems is based on manmade polymers.[14] Not only that they are not biocompatible but also may exhibit toxicity. As a consequence, they cannot be used for biomedical applications. It is, therefore, of particular importance to develop a novel method to anchor CuONPs onto composites derived from biocompatible and sustainable macromolecules, such as cellulose (CEL), chitosan (CS), and keratin (KER).

We have demonstrated recently that a simple ionic liquid (IL), butylmethylimmidazolium chloride ([$BMIm^+Cl^-$]), can dissolve CEL, CS, and KER. With this IL as the only solvent, we developed a simple, green, and totally recyclable method to synthesize [CEL + CS] and [CS + KER] [CEL + CS/KER] composites by just dissolving the biopolymers in the IL without chemical modification.[15-21] Results of Fourier transform infrared (FTIR), near-infrared, X-ray diffraction (XRD), and ^{13}C cross polarization magic angle spinning–NMR measurements indicated no change in the structures of CEL, CS, and KER.[15-21] The [CEL + CS/KER] composites were biocompatible and fully retained unique properties of their constituents, i.e., superior mechanical strength (from CEL), antibacterial activity (from CS and KER), and controlled release of drugs (from KER).[15-21]

These data clearly indicate that [CEL + CS/KER] is particularly suited as a biocompatible composite to encapsulate CuONPs to prevent the NPs from aggregation, coagulation, and leaching, thereby allowing them to render reproducible antibacterial and antiviral activity. Such considerations prompted us to fully exploit advantages of IL, a green solvent, to develop a novel and simple method to synthesize [CEL + CS/KER] composites containing CuONPs. Because the [CEL + CS/KER + CuONPs] composites prevent aggregation, coagulation, and changes in the size and morphology of CuONPs, the unique property of the nanoparticles is fully retained for repeated and reproducible use without any complication of reducing activity. We report, in this study, the synthesis of [CEL + CS/KER + CuONPs] composites and characterize their structure using FTIR, electron paramagnetic resonance (EPR), XRD, scanning electron microscopy (SEM), and energy-dispersive spectroscopy (EDS) techniques. We also systematically carried out bioassays to

determine antimicrobial activity and biocompatibility of the [CEL + CS + CuONPs] composites. Results obtained are reported in this study.

Experimental Section

Chemicals

Cellulose (microcrystalline powder) and chitosan (molecular weight ≈310–375 kDa) were the same as those used in our previous studies.[15-17] They were obtained from Sigma-Aldrich (Milwaukee, WI) and used as received. Raw (untreated) sheep wool was obtained from a local farm. It was purified using a method previously used in our laboratory.[17-19] That is, it was cleaned by Soxhlet extraction using a 1:1 (v/v) acetone/ethanol mixture at 80 ± 3 °C for 48 h, followed by rinsing with distilled water and drying at 100 ± 1 °C for 12 h.[17-19] [$BMIm^+Cl^-$] was synthesized from 1-methylimidazole and *n*-chlorobutane (both from Alfa Aesar, Ward Hill, MA) as previously reported.[15-21] Copper(II) oxide (CuO, purity >99%) was bought from Acros Organics and used as received. Biochemicals, including nutrient broth (NB) and nutrient agar (NA), minimal essential medium, fetal bovine serum (FBS), penicillin–streptomycin, Dulbecco's modified Eagle's medium (DMEM), phosphate-buffered saline (PBS), trypsin solution (Gibco), and CellTiter 96 AQueous One Solution Cell Proliferation Assay were obtained from the same sources as previously reported.[19]

Instruments

Instruments used in this study were the same as those used previously.[15-19] Specifically, FTIR spectra were recorded from 450 to 4000 cm^{-1} and with 2 cm^{-1} resolution on an FTIR spectrometer (Spectrum 100 Series, PerkinElmer) using the KBr method. Each spectrum was an average of 64 individual spectra. X-ray diffraction (XRD) measurements were taken on a Rigaku MiniFlex II diffractometer equipped with Ni-filtered Cu Kα radiation (1.54059 Å). The X-ray tube was operated at 30 kV and 15 mA. The samples were measured within the 2θ range of 2.0–80.0°. The scan rate was 5°/min. The Jade 8 program was used to process the data package. The surface and cross-sectional morphologies of the composite films were recorded under vacuum with a JEOL JSM-6510LV/LGS scanning electron microscope with standard secondary electron and backscatter electron detectors. The composites were initially made conductive by applying a 20 nm gold–palladium coating onto their surfaces using an Emitech K575x Peltier Cooled Sputter Coater (Emitech Products, TX). A Misonix Sonicator (Farmingdale, NY) model 3000 was used to disperse CuO powder in ionic liquid.

Procedure Used To Determine Concentration of Copper in [CEL + CS + CuONPs] Composites

The amounts of copper (Cu) in [CEL + CS + CuONPs] composites were determined by both flame atomic absorption spectrometry (AAS, PerkinElmer AAS 3100) and inductively coupled plasma-mass spectrometry (ICP-MS) (Agilent 7700 (G3281A) ICP-MS). Reported procedure with minor modification was used to digest CuONP composites for AAS and ICP-MS measurements.[22] Specifically, the composite samples were digested by suspending 50.0 mg of sample in 50.0 mL of double-distilled water containing 1 mL of 11.0 N sulfuric acid and 0.400 g of ammonium persulfate. The mixture was boiled gently on a hot plate until the final volume reached 10 mL. This took ca. 3/2 h. CuONPs in the composite dissolved completely during this process. The solution was allowed to cool and then diluted to 30.0 mL with double-distilled water. The solution was then neutralized with

1.0 N NaOH with phenolphthalein as an indicator. The resulting solution was then diluted to 100 mL and used as stock solution for the determination of Cu by both flame AAS and ICP-MS.

The stock solution prepared from the digested solution was diluted further to 100 mL with double-distilled water. Standard addition method was used to determine the copper concentration in the sample. Specifically, 10 mL of this dilute sample solution was pipetted into each of the 6 × 25 mL volumetric flasks. Various amounts (0.0–5.0 mL) of 10.0 ppm Cu^{2+} were systematically added to the flasks, and the volume of each flask was adjusted to 25 mL with 0.2 M HNO_3 solution. The atomic absorbance of copper in each solution was then measured at 324.75 nm on a flame atomic absorption spectrometer (PerkinElmer AAS 3100) with air and acetylene used as oxidant and fuel, respectively. For ICP-MS measurements, 0.5 mL of the stock solution was further diluted to 100 mL with an aqueous solution of 2% HNO_3 and 0.5% HCl v/v. The diluted samples were then analyzed on an ICP-MS instrument.

Electron Paramagnetic Resonance

EPR spectra were recorded at 23 ± 1 °C, 9.84 GHz, 4 mW microwave power (nonsaturating), and 6 G (0.6 mT) field modulation amplitude at 100 kHz, on an updated Bruker EMX-TDU/L spectrometer, equipped with an ER4116DM resonator and an EIP 548A microwave frequency counter. Other acquisition parameters were chosen such that the spectral resolution (~2 G) was determined by the modulation amplitude. Composite samples (each with dimension of 30 mm × 3 mm and approximate weight of 5 mg) were placed between the flat planes of two acrylic semicylinders with r = 3 mm, and the entire assembly was mounted in the open end of a 4 mm o.d. quartz EPR tube (707-SQ-250M, Wilmad). The assembly was rotated in the tube so that the plane of the film is aligned with a taped flag on the EPR tube, which was then used to orient the sample in the field with a rotating collet. AAS and ICP-MS results show that the samples were each of nominal total mass 5 mg and contained either 20, 35, 85, or 140 μg Cu per 5 mg of each CEL/CS composite.

EPR signals due to Cu(II) were quantified by double integration relative to a sample of 0.7 mM Cu(II)–ethylenediaminetetraacetate (EDTA) in *N*-(2-hydroxyethyl)piperazine-*N*′-ethanesulfonic acid buffer, pH 7.0, recorded under nonsaturating conditions (0.2 mW) at 77 K, with the usual corrections for T^{-1}, (microwave power)$^{1/2}$, and $(\Delta B)^{-2}$. The experimental signals from the composites were first baseline-normalized by subtraction of a linear background that equalized the area above and below the baseline and then doubly integrated (Xenon, Bruker Biospin) to estimate the total number of spins due to EPR-detectable Cu(II). The broad signal was then removed by fitting and subtracting a polynomial (typically fifth order), and the narrow tetragonal signal around g = 2 was doubly integrated to estimate the amount of monomeric Cu(II). The number of spins due to the broad signal was then taken as the difference of the overall and tetragonal Cu(II) intensities.

Computer modeling of the orientation dependence of the EPR spectra of [CEL + CS + CuONPs] was carried out using simulations generated with EasySpin 5.1.10.[(23)] Parameters for the spectra were estimated by powder simulation of spectra obtained with [CEL + CS + CuONPs] composite film perpendicular to the scanned magnetic field. Spectra were then calculated using different values of the “ordering parameter” in EasySpin, where

$$P(\theta) = \exp -U(\theta) \quad (1)$$

And

$$U(\theta) = -\lambda[(3\cos^2\theta - 1)/2] \quad (2)$$

Here, λ determines the sharpness of the distribution and θ is the angle between the molecular *z* axis and the magnetic field. When it is known that the sample is completely directionally ordered, EasySpin simulations can provide the orientation of the molecules with respect to the sample geometry. Alternatively, as in the present case, the ordering parameter can be used to estimate the extent of directional ordering in a sample for which the sample orientations for the most single-crystal-like EPR spectra have been determined. An ordering parameter of zero corresponds to no orientation dependence of the spectrum (i.e., the powder spectrum). A negative ordering parameter corresponds to selective orientation of $g_{||}$ of directionally ordered Cu(II) in the direction of the scanned magnetic field ($\mathbf{B}_0$), and a positive ordering parameter corresponds to selective orientation of the $g_{\perp}$ plane of directionally ordered nominally tetragonal Cu(II) in the direction of the scanned magnetic field. The orientation-dependent computer simulations were used to correlate the ordering parameter to the experimentally accessible ratio of the intensities of the lowest-field $m_I = {}^3/_2$ $A_{||}(^{63/65}\mathrm{Cu})$ hyperfine line and the highest-field feature, the extra-absorption line that arises in powder spectra due to the different orientation dependencies of $A_{||}$ and $g_{||}$ for tetragonal Cu(II).[(24)] This approach provided a method by which the extent of direction-selective orientation of Cu(II) by the films was estimated from the experimental EPR data from films oriented in the magnetic field.

Antibacterial Assays

In separate experiments, American Type Culture Collection (ATCC) strains of *E. coli*, methicillin-resistant *S. aureus* (MRSA), and *Pseudomonas aeruginosa*, as well as clinical strains of *E. coli* possessing an extended-spectrum β-lactamase enzyme (highly resistant *E. coli*), *Enterobacter cloacae*, *Proteus mirabilis*, *Stenotrophomonas maltophilia*, *Candida albicans*, vancomycin-resistant *Enterococcus* spp. (VRE), and *Streptococcus agalactiae*, were initially propagated on tryptic soy agar with 5% sheep erythrocytes (Remel, Lenexa, KS) overnight in 35 °C ambient air. Isolated colonies were subcultured into 3 mL cultures of nutrient broth (Remel) and incubated in 35 °C ambient air.

A 3 μL aliquot of overnight broth culture was aseptically transferred into individual 3 mL tubes of nutrient broth. Tube contents were vortexed to produce a homogeneous suspension of organisms. [CEL + CS + CuONPs] composite strips (20 mm × 3.5 mm) and control strips ([CEL + CS] composite) were added to respective culture tubes. Prior to 35 °C ambient air incubation, a 50 μL aliquot was removed from the broth cultures and transferred into sterile microcentrifuge tubes. Aliquots were serially 10-fold diluted in triplicate utilizing nutrient broth, and 100 μL aliquots of selected dilutions were spread onto nutrient agar (Remel) plates and incubated overnight in 35 °C ambient air. Enumeration of colonies failed to reveal significant differences between the two treatment groups (data not illustrated), signifying a standardized initial inoculum for all cultures.

Following 16 h incubation, broth cultures with added [CEL + CS ± CuONPs] composite were vortexed for 10 s, and 50 μL aliquots were removed and transferred into sterile microcentrifuge

tubes. Tube contents were vortexed and serially 10-fold diluted in triplicate. The 100 µL aliquots of selected dilutions were spread onto nutrient agar plates and incubated overnight in 35 °C ambient air. Plates that yielded between 30 and 300 colonies were the basis for colony enumeration. Triplicate results from a given treatment group were averaged. Mean data derived from [CEL + CS + CuONPs] composite were compared to control ([CEL + CS] composite) for calculation of $\log_{10}$ growth reduction.

Biocompatibility Assays

Low-passage (<3) ATCC CRL-2522 fibroblast cell lines were cultivated for 14–21 days in tissue culture-treated vented flasks. The cells were maintained at 35 °C in a 5% CO_2 atmosphere, in Dulbecco's modified Eagle's medium (DMEM) with 4.5 g/L glucose and 4.5 g/L l-glutamine (Corning, Manassas, VA), supplemented with 10 000 U/mL penicillin, 10 mg/mL streptomycin (Sigma-Aldrich, St. Louis, MO), and 10% fetal bovine serum (Atlanta Biologicals, Norcross, GA). Adherent fibroblasts were dissociated with 2 mL 0.25% trypsin–EDTA, phenol red (Thermo Fisher Scientific), and 30 min incubation at 35 °C in 5% CO_2. Subsequent nonadherent fibroblasts were transferred into a 50 mL sterile centrifuge tube and concentrated (200*g*, 10 min, 23 °C). Pellets were resuspended in 2 mL fresh DMEM, and fibroblasts were enumerated by hemacytometry.

The 2×10^4 fibroblasts in 2 mL of fresh DMEM were added to individual wells of 24-well tissue culture plates (Thermo Fisher Scientific). Three wells were set aside for incubation of 2 mL additions of DMEM alone. Cultures were incubated overnight at 35 °C in 5% CO_2. Medium was aspirated from each well and replaced with 2 mL of fresh DMEM. Disks (10 mm diameter) of composites with or without copper oxide ([CEL + CS ± CuONPs]) were added to fibroblast culture wells in triplicate; additional three fibroblast culture wells received no additives and served as a mock control.

Following 72 h incubation at 35 °C in 5% CO_2, the composite disks were aseptically removed, culture contents were aspirated, and the culture wells were washed with successive 2 and 1 mL aliquots of 1× PBS, pH 7.4 (Thermo Fisher), to remove nonadherent cells. A small amount (1 mL) of 0.45 µm filtered DMEM without phenol red (Sigma-Aldrich) supplemented with 10% fetal bovine serum was delivered to each well of the 24-well plate. Proliferative activity was assessed by the addition of 200 µL of a 1:20 solution of electron coupling reagent (phenazine methosulfate)/novel tetrazolium compound (3-(4,5-dimethylthiazol-2-yl)-5-(3-carboxymethoxyphenyl)-2-(4-sulfophenyl)-2*H*-tetrazolium) solution (CellTiter 96 AQ_{ueous} Non-Radioactive Cell Proliferation Assay; Promega, Madison, WI) to each well. Following 3 h incubation (35 °C, 5% CO_2), 500 µL of culture aliquots was removed and concentrated (14 000 rpm, 1 min, 23 °C). A_{490} of 100 µL supernatants was determined by spectrophotometry (Molecular Probes).

The mean A_{490} value derived from the three DMEM wells was subtracted from remaining wells containing fibroblasts and/or composite derivatives. Mean-adjusted A_{490} data and standard error of the mean were computed for triplicate fibroblast culture treatments. Remaining medium was aspirated from wells for photomicrograph imaging of cell monolayers.

Results and Discussion

Synthesis of [CEL + CS/KER + CuO] Composites

[CEL + CS + CuONPs] composites were synthesized with minor modification to our previously used procedure for the synthesis of [CEL + CS] composites.[15-19] In essence, as shown in Scheme 1, [$BMIm^+Cl^-$] was used to dissolve CEL and CS under vigorous stirring at 100 °C under an argon atmosphere. All polysaccharides were added in portions of ~1 wt % of the total ionic liquid used. Each portion was added only after the previous addition had completely dissolved until reaching the desired concentrations. In a separate flask, CuO powder was dispersed in a copious amount of [$BMIm^+Cl^-$] (~7 g) by sonicating at 100 °C and 5 W power on a Misonix Sonicator for 1 h prior to adding to the solution of [CEL + CS] in [$BMIm^+Cl^-$]. Using this procedure, [$BMIm^+Cl^-$] solutions of [CEL + CS + CuO] with various proportions and concentrations of CuO powder (3, 5, 10, 20, and 37 mg) were prepared in about 6–8 h. The resulting solutions were then cast on Mylar sheets and homemade poly(tetrafluoroethylene) molds of the desired size and thickness (e.g., 38 mm (*W*) × 45 mm (*L*) × 0.8 mm (*H*)). They were then kept at room temperature for 24 h to allow gelation to yield GEL films. The [$BMIm^+Cl^-$] in the films was removed by washing the films with water for about 4 days. During this period, the wash water was constantly replaced every 8 h with fresh deionized water to facilitate complete removal of the ionic liquid. Water from the washed aqueous solution was then distilled away, leaving remaining [$BMIm^+Cl^-$] for reuse. The regenerated composite films were then oven-dried at 60 °C for about 48 h to yield dried composite films (DRY films). By replacing CS with wool, [CEL + KER + CuONPs] composites with different concentrations of CuONPs were prepared. Because it is possible that not all added CuO powder would remain in the composites, actual amounts of copper in the composites were determined by digesting the composites in mineral acid solution for subsequent measurements by both flame AAS and ICP-MS. Actual amounts of copper in the composites, found by both methods, were the same within experimental error. That is, for 5.0 g of [CEL + CS + CuONPs] composites, prepared with 3, 5, 10, 20, and 37 mg of added CuO powder, the actual amounts of copper were found to be 1.12, 1.87, 3.40, 8.36, and 13.69, respectively. The results indicate that about 47% of added CuO was encorporated as CuONPs in the composites.

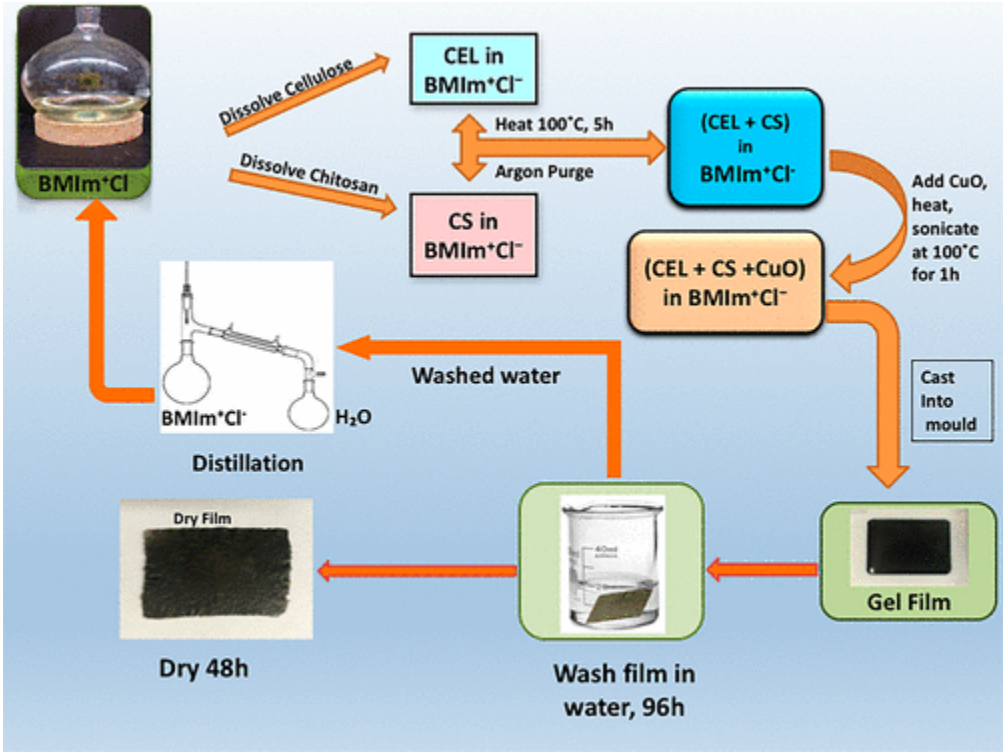

Scheme 1. Procedure Used To Prepare the [CEL + CS + CuONPs] Composites

Structure of the [CEL + CS/KER + CuONPs] Composites

FTIR

The FTIR spectrum of the [CEL + CS] composite, shown as the black trace in Figure 1, is similar to the spectrum previously obtained for [CEL + CS] composite. Specifically, bands correspond to stretching vibrations of O–H, C–H, and −O– groups in both CEL and CS are evident at around 3400, 2850–2900, and 890–1150 cm^{-1}, respectively.[15-18] Additionally, the presence of CS also produces bands at around 3400, 1657, 1595, and 1300–1200 cm^{-1}, which can be tentatively assigned to the symmetric and asymmetric N–H stretching, C═O, amide 1, NH deformation, and the in-phase N–H bending, respectively.[15-18] Also shown in red is the spectrum for [CEL + CS + 35 nmol/mg CuONPs] composite (i.e., 0.5 g of composite with 1.12 mg of copper). The fact that the red spectrum of the [CEL + CS + 35 nmol/mg CuONPs] composite is relatively similar to the black spectrum of the [CEL + CS] composite suggests that there may not be strong interaction between the CuONPs and CEL and CS in the composite. However, careful inspection of the spectra revealed that there are indeed minor differences in the amino bands. Specifically, it seems that interaction between CuO and N–H groups (of CS) leads to the shift in the symmetric and asymmetric N–H stretching band from 3423.0 cm^{-1} ([CEL + CS]) to 3412.0 cm^{-1} ([CEL + CS + 35 nmol/mg CuONP]) and a shift in the C–N band from 1320.5 cm^{-1} ([CEL + CS]) to 1319.5 cm^{-1} ([CEL + CS + 35 nmol/mg CuONPS]). These results suggest interactions between the Cu and the amino groups of CS.

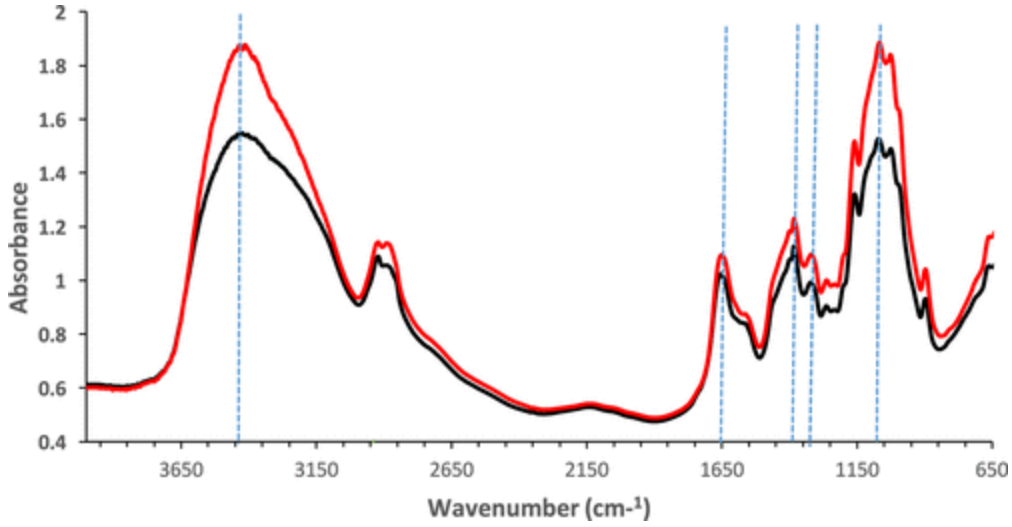

Figure 1. FTIR spectra of [CEL + CS] composite (black) and [CEL + CS + 35 nmol/mg CuONPs] composite (red).

X-ray Diffraction (XRD)

X-ray diffractograms of [CEL + CS] and [CEL + CS + 434 nmol/mg CuONPs] composites are shown in Figure 2. Because CEL and CS are present in both composites, it is as expected that both spectra have similar two broad bands at around 2θ = 10.45 and 20.50°. These bands are the same as those observed previously for [CEL + CS] composite. As expected, adding 434 nmol/mg of CuONPs into the composite leads to several narrow crystalline bands, and the three most pronounced bands are at around 2θ = 35.57, 38.77, and 48.82°. These bands are similar to those previously reported for CuONPs and also to bands in the reference diffractogram of CuO in JCPDS 048-1548.[25-28] They can, therefore, be assigned to the (−1 1 1), (1 1 1), and (−2 0 2) bands of CuO, respectively. Together, the results clearly indicate that copper oxide is present as CuONPs in the [CEL + CS + CuONPs] composite.

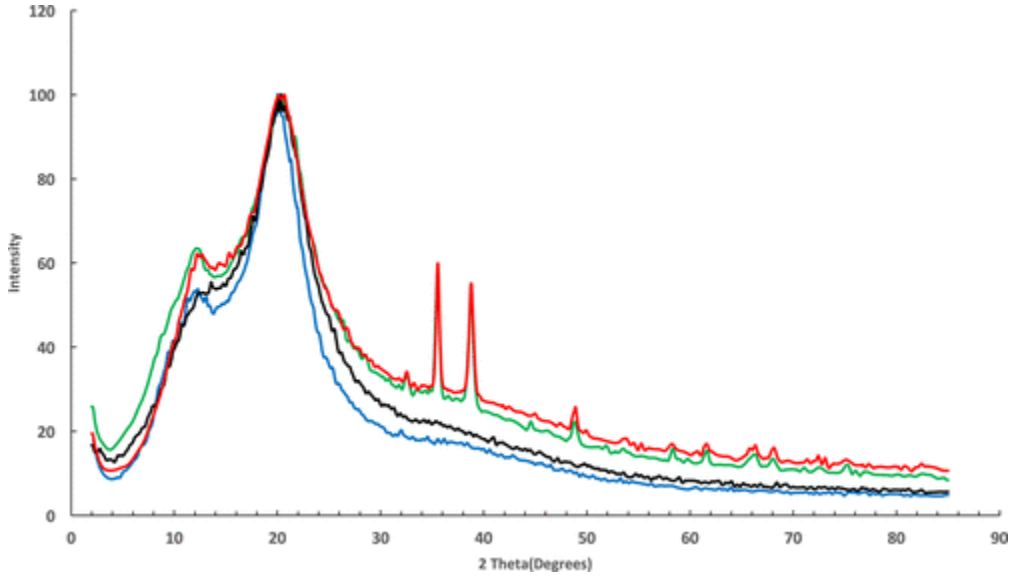

Figure 2. Powder X-ray diffractograms of [CEL + CS] composite (blue), [CEL + CS + 434 nmol/mg CuONPs] composite (red), [CEL + KER] composite (black) and [CEL + KER + 434 nmol/mg CuONPs] composite (green).

The size (τ value) of the CuONPs in the composite was then calculated using the Scherrer equation from the full width at half-maximum (β value in the equation) of the corresponding XRD bands[29, 30]

$$\tau = \frac{k\lambda}{\beta \cos\theta} \quad (3)$$

where τ is the size of the nanoparticle, λ is the X-ray wavelength, and *k* is a constant.[29, 30] The size of the copper oxide nanoparticle in the [CEL + KER + 434 nmol/mg CuONPs] composite was found to be (22 ± 1) nm.

SEM Images and Energy-Dispersive Spectroscopy (EDS) Analysis

Figure 3A,B shows, respectively, the surface and cross-sectional SEM images of [CEL + CS + 298 nmol/mg CuONPs] composite. As expected, these images are similar to those reported previously for [CEL + CS] composite, namely, the composite is homogenous and has a somewhat fibrous structure.[15-19] This is likely imparted by CEL, which itself has a fibrous structure. More information on the chemical composition and homogeneity of the CuONPs can be found in the EDS image and spectrum shown in Figure 3C,D, respectively. Figure 3C, which is EDS image recorded for copper, clearly indicates that CuONPs are homogeneously distributed throughout the composite. The EDS spectrum (Figure 3D) shows two major bands at around 284 and 531 eV due to carbon and oxygen (of CEL and CS in the composite) and the third major band at 933.5 eV that is assigned to Cu(II) oxide based on those reported previously for CuO[25-28] (the two minor bands due to Au and Pd are from coating of the composite with gold and platinum to facilitate SEM measurements).

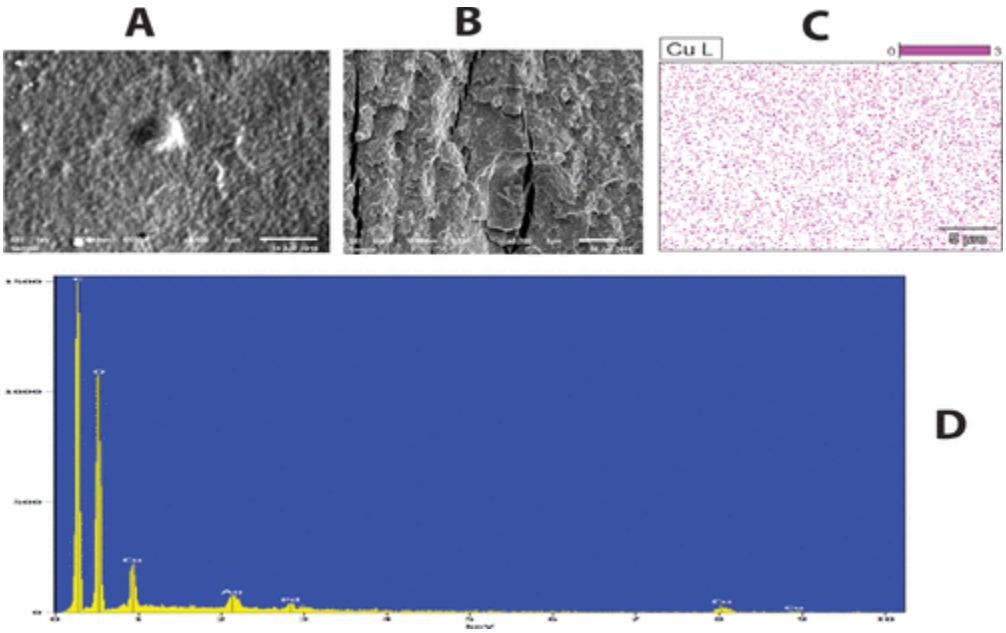

Figure 3. (A) Surface SEM image and (B) cross-sectional SEM image of [CEL + CS + 108 nmol/mg CuONPs]; (C) EDS image of composite recorded for copper; and (D) EDS spectrum of the composite.

Electron Paramagnetic Resonance (EPR)

EPR spectra of films of the composites [CEL + CS + CuONPs] and [CEL + KER + CuONPs] are shown in Figure 4, with 140 μg of Cu per 5 mg of composite, along with spectra from CuO powder and a film of the [CEL + CuONPs] composite for comparison. The films were oriented either parallel or perpendicular to the scanned magnetic field (pictographic notations]–[and] | [will be used for parallel and perpendicular orientation in the $\mathbf{B}_0$ field, respectively, where the brackets represent the pole pieces of the magnet and the center symbol represents the film), and spectra in both orientations are shown. The spectra for CuO (A) and [CEL + CuONPs] (B) were extremely broad due to extensive spin-interaction between Cu(II) ions, although some orientation dependence of the signal from [CEL + CuONPs] was observed. The spectra from [CEL + CS + CuONPs] (C) and [CEL + KE + CuONPs] (D) also contained a broad component, similar but by no means identical to CuO and [CEL + CuONPs] but were dominated in the traditional first derivative ($\partial\chi''/\partial B$) display by signals typical of tetragonal Cu(II), with well-resolved $m_I = |^3/_2\rangle$ and $m_I = |^1/_2\rangle$ resonances due to the four-line $I = {}^3/_2$ $A_{||}(^{63/65}\mathrm{Cu})$ hyperfine manifold, at around 2900 and 3100 G, respectively, and an intense feature at 3400–3500 G that is due to the superposition of the $g_\perp$ and the extra-absorption resonances.[24, 31] Despite the higher peak-to-trough amplitude of the tetragonal signal, careful integration showed that 75% of the Cu(II) was present as the broad species, and only 25% due to the tetragonal species. For well-resolved spectra, geometrical information is readily available from EPR of Cu(II).[32-37] Briefly, for tetragonal and related square-planar-based geometries, an essentially axial spectrum is expected with $g_{||} > g_\perp > 2$. A highly axial hyperfine interaction with the $I = {}^3/_2$ ^{63}Cu or ^{65}Cu nucleus is manifested as a splitting of the $g_{||}$ resonance into four lines, of which either three or four are typically resolved at X-band, depending on the coordination and its effect on the spin-Hamiltonian parameters. These types of spectra, as observed here for [CEL + CS + CuONPs] and [CEL + KS + CuONPs], are a consequence of the

nominally d$x^2 - y^2$ ground-state paramagnetic orbital (better described as d$x^2 - y^2$/dxy for lower than ideal symmetry). Severe distortion of tetragonal geometry introduces mixing of the dz^2 orbital into the paramagnetic orbital, which would result in a now rhombic **g** tensor, with $g_z > g_y > g_x \cong 2$ and $A_z > A_x \gg A_z$, where a four-line pattern is typically only resolved in the *z* and *x* orientations (lowest- and highest-field electronic Zeeman resonances, respectively) at X-band. For geometries with a formal dz^2 paramagnetic ground state, most notably trigonal bipyramidal, $g_\perp > g_\parallel = 2.0$. No evidence for the latter two cases was observed, and we conclude that the Cu(II) species that dominates the $\partial\chi''/\partial B$ EPR spectra and accounts for 25% of the total spins of [CEL + CS + CuONPs] and [CEL + KER + CuONPs] are (i) essentially tetragonal, (ii) uncontaminated by significant inter-Cu(II) spin–spin exchange coupling, and (iii) highly distinct from the spectra of CuO in either powder form or associated with CEL. These particular Cu(II) EPR signals from [CEL + CS + CuONPs] and [CEL + KER + CuONPs] are presumably, therefore, due to copper binding that is mediated by the CS and KE complements, respectively, of the substrates.

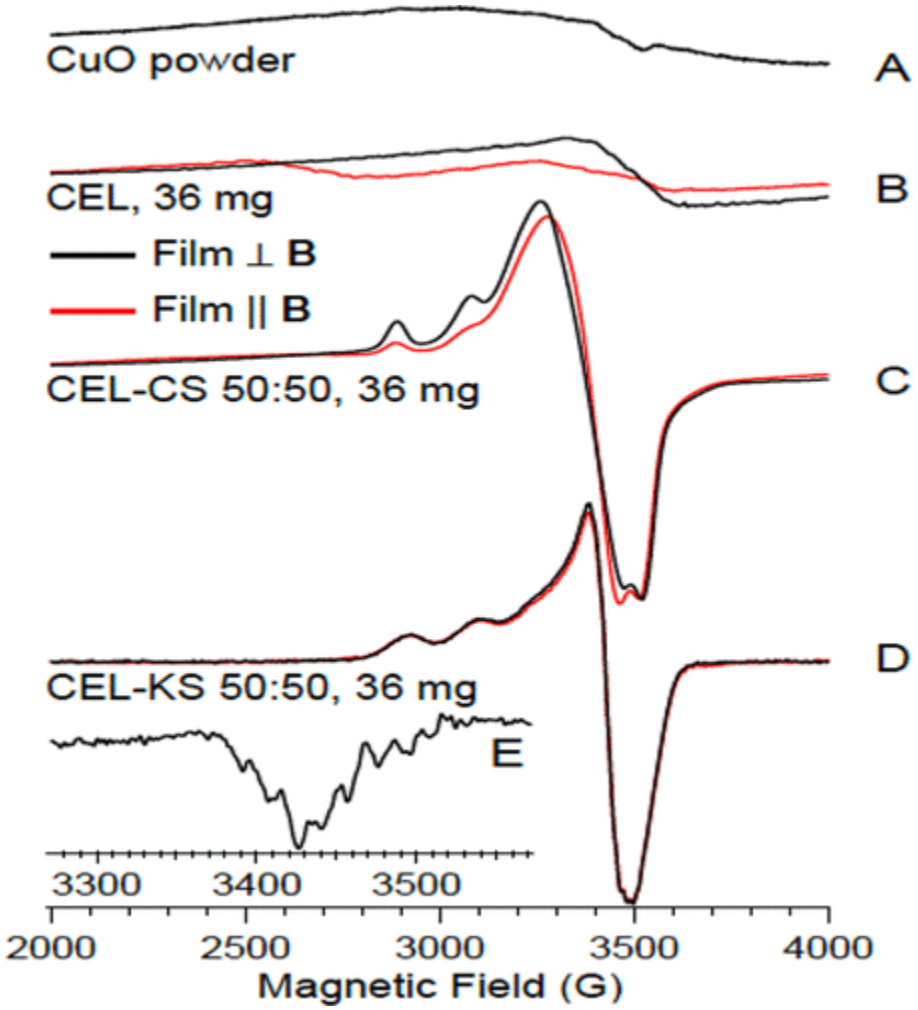

Figure 4. EPR spectra of CuO powder and CEL, 50:50 [CEL + CS] and 50:50 [CEL + KE] composites with CuONPs: (A) CuO powder; (B) CEL composite with 140 μg of Cu; (C) [CEL + CS] composite with 140 μg of Cu; and (D) [CEL–KE] composite with 140 μg of Cu. The inset (E) is the second-derivative ($\partial^2\chi''/\partial B^2$) display of the $g_\perp$ region of the spectrum of [CEL + KE + CuNPs] composite,

revealing $^{63/65}$Cu hyperfine and/or ^{14}N superhyperfine structure. Spectra are shown with the composites oriented both parallel (red curves) and perpendicular (black curves) to the scanned magnetic field.

The spectrum from [CEL + KER + CuNPs] exhibited additional hyperfine structure in the $g_{\perp}$ region with A = 15 G and containing at least eight lines and with $A_x \approx A_y$, suggestive of coupling to multiple ^{14}N nuclei, but it did not display any dependence on the orientation of the film in the field. In contrast, the signal from [CEL + CS + CuONPs] was markedly orientation-specific. As the sample was rotated from the] | [orientation to the]–[orientation, the intensity of the $A_{||}$ hyperfine lines diminished progressively. Additionally, the broad underlying signal exhibited a similar orientation dependence to that from [CEL + CuONPs]. The maximum and minimum intensities of the $A_{||}$ hyperfine lines were observed at the] | [and]–[film orientations, respectively. No x–y orientation dependence in the plane of the film of the EPR spectra was observed, consistent with essentially tetragonal Cu(II), with $g_x = g_y$.

The relative and absolute intensities of the EPR signals from [CEL + CS + CuONPs] were surprisingly insensitive to the amount of copper, estimated by flame AAS and ICP-MS, over the range 20–140 μg per 5 mg of composite, and to the composite ratio of CEL/CS, across the range 25:75–75:25. The absolute signal intensities corresponded to 0.35 ± 0.06 μmol Cu(II), and the proportion of the signal due to the monomeric tetragonal species was 29 ± 7%. At lower proportions of CS, the intensities of the EPR signals were (i) much less intense overall, (ii) of highly varying intensities between batches of composite, and (iii) of highly varying proportions of the tetragonal species. Analogous irreproducibility was observed between batches of material prepared with ≤0.2 μmol Cu(II) per 5 mg substrate. These samples, with low [CS] and/or ≤40 nmol/mg Cu, and no reproducibility of EPR-detectable amounts of Cu(II) and Cu(II) speciation, were not studied further.

The EPR quantitation of Cu(II) differs markedly from analytical estimates of total copper and suggests that a significant proportion of the copper in composite prepared with >59 nmol/mg is EPR-silent. This is not too surprising, given that much of the Cu(II) in nanoparticles is likely to exhibit extensive spin–spin interactions with its neighboring Cu(II) ions, which result in a diamagnetic ground state. The tetragonal copper is due to magnetically isolated Cu(II) ions that have not grown into nanoparticles. The structure of this copper species is important, however, as it provides information on how copper is first anchored to the composite substrate and provides a rationale for the stability of the copper nanoparticle–composite system that is crucial for biomedical application. The broad EPR signal is perhaps due to smaller CuONPs and/or Cu(II) on the surface of larger CuONPs. As more copper is added and the CuONPs grow in size, deeply buried Cu(II) is likely rendered EPR-silent by the extensive spin–spin interactions, which may either thermodynamically isolate the diamagnetic ground state (i.e., increased spin-coupling-determined zero-field splitting, D_J) or provide additional pathways for very fast relaxation of thermally accessible excited $S > 0$ spin states, or both. The EPR data, therefore, appear to provide insight into copper adsorption and binding to substrate and subsequent evolution of CuONPs.

In addition to the likely coordination sphere of the copper anchor, EPR also provides information on orientation. Figure 5 shows spectra of [CEL + CS + CuONPs] composites prepared with different amounts of added CuO in both orientations, and in both the first- ($\partial\chi''/\partial B$; A–C) and second-derivative ($\partial^2\chi''/\partial B^2$; D–F) displays. The orientation-dependent difference in the intensities of the

$A_\perp$($^{63/65}$Cu) manifolds in each of the sets of spectra is immediately clear. However, a closer inspection of the $g_\perp$ region of the $\partial^2\chi''/\partial B^2$ spectra of Figure 5 reveals a clear hyperfine pattern that is markedly dependent on the orientation of the film in the magnetic field (shown in detail in Figure SI-1 and explained in text in the Supporting Information). Six lines are clear, centered at 3400 G, and correspond to the genuine $A_\perp$ manifold (as opposed to the extra-absorption line) with a splitting of 13.5 G. Further points of inflection continue into the extra-absorption line to higher field, but this pattern is less clear as the two regions overlap. The $A_\perp$ hyperfine pattern is strongly reminiscent of those exhibited by other Cu(II) systems with multiple nitrogen ligands and, though in itself not definitive, is highly suggestive of multiple nitrogen ligands of Cu(II) in [CEL + CS + CuOPNs].[31] Supporting evidence for multiple nitrogen ligation of copper in both [CEL + CS + CuONPs] and [CEL + KER + CuONPs] arises from a Peisach and Blumberg analysis of the EPR spectra of these species, which indicates that the Cu(II) responsible for the hyperfine-split signal is coordinated by at least two nitrogen atoms (Figure SI-2).[38] A final piece of evidence for ligation of copper by nitrogen in [CEL + CS + CuONPs] comes from varying the ratio of CEL to CS (Figure SI-3). In the composite with higher CEL content (75:25 CEL/CS; trace F of Figure SI-3), the hyperfine structure in the $g_\perp$ region is relatively weak, whereas the putative ^{14}N hyperfine pattern is very clearly resolved for composite with higher relative CS content (25:75 CEL/CS; Figure SI-3, trace D), where the number of nitrogen atoms available for copper coordination is expected to be three times higher than with only 25% CS.

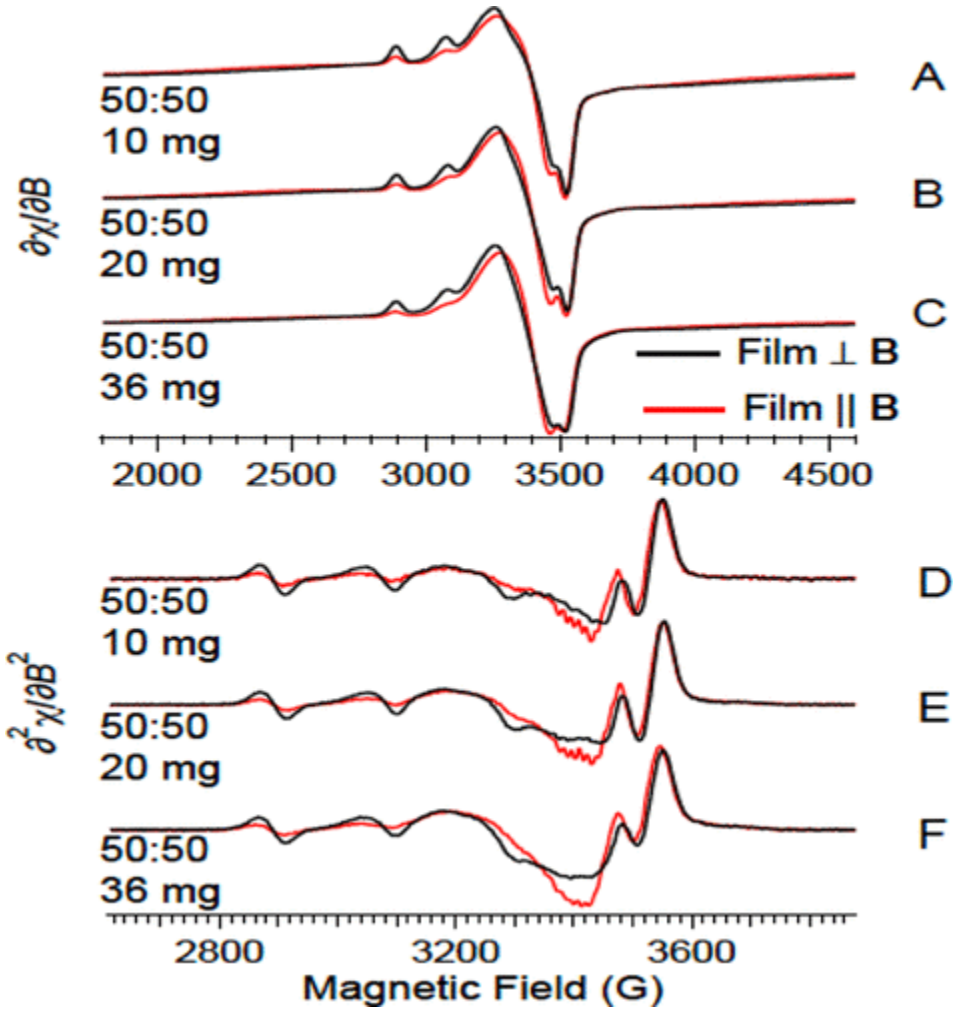

Figure 5. Selected EPR spectra of 50:50 [CEL + CS] composites with different CuONP contents. Spectra are shown with composites oriented both parallel and perpendicular to the scanned magnetic field, in the first derivative ($\partial\chi''/\partial B$) (A–C) and the corresponding second derivative ($\partial^2\chi''/\partial B^2$) (D–F). Intensities have been normalized.

In an analogous study of DNA fibers to which Cu(II) complexes of phenanthroline were bound,[(39)] fibers could be oriented to exhibit single-crystal-like EPR spectra with pure parallel or perpendicular resonances at particular orientations. This phenomenon allowed calculation of the orientation of the complexes with respect to the fiber axis. In the present study, no orientations of the film in the magnetic field could be found for which pure single-crystal-like EPR spectra could be obtained. This is perhaps not surprising given the heterogeneity of the fiber orientation of [CEL + CS] observed in the electron micrograph (Figure 3B). Here, then, the goal was to use the ordering parameter of the orientation-dependent spectra to determine the extent of orientation of the copper in [CEL + CS + CuONPs], rather than the direction of orientation itself in detail.

Spin-Hamiltonian parameters for the powder spectrum of [CEL + CS + CuONPs] were estimated from the experimental spectrum of Figure 5C with the film in the] | [orientation. These parameters were then used to calculate spectra with ordering parameters varying from −10 (red trace of Figure

SI-4), corresponding to the orientation of the $g_{||}$ direction along the scanned magnetic field, to +4 (blue trace of Figure S4), corresponding to the orientation of the $g_{\perp}$ plane along the scanned magnetic field; an ordering parameter of 0 corresponds to the powder spectrum. The ratios of the intensities of the features labeled A and B in Figure S4 were then plotted against the ordering parameter (inset, Figure S4), and the curve was used to determine the ordering parameters for experimental spectra of [CEL + CS + CuONPs] (Figure SI-5). The values for the experimental spectra differed only slightly, and in most cases within or close to experimental reproducibility, depending on the amount of copper in [CEL + CS + CuONPs] or on the CEL/CS ratio, consistent with the overall similarity of the spectra themselves. The ordering parameters for the] | [orientation were close to those expected for disoriented powder spectra, indicating significant projections of both the $g_{||}$ direction and the $g_{\perp}$ plane along the applied magnetic field. In contrast, the ordering parameters for the]–[orientation of the film were in the +1.5 to +2.0 range, which, by inspection of the computed spectra and correlation curve of Figure S4, indicates that there is little projection of the $g_{||}$ direction along the applied magnetic field with the film in that orientation.

The EPR data indicate, then, that Cu(II) binds in three distinct environments. A small amount of composite (5 mg) can bind up to ∼18.7 μg of Cu(II) as detectable paramagnetic species. Beyond 18.7 μg of copper, no increases in the EPR signal intensities are observed, presumably due to large nanoparticle formation with extensive spin–spin interactions. The broad signal, corresponding to about 75% of the observable Cu(II), is clearly due to more than one interacting Cu(II) ions, and is likely due to either small protonanoparticles and/or surface Cu(II) on larger nanoparticles. The remaining 25% is a monomeric species with a clearly defined hyperfine structure and, for [CEL + CS + CuONPs], an orientation dependence. The data establish that this monomeric species is a product of binding by the CS or KER complement, respectively, of [CEL + CS + CuONPs] and [CEL + KER + CuONPs], and are indicative of binding by multiple nitrogen atoms in the equatorial plane of the tetragonal Cu(II) ion (EPR indicates either 2 or 3, although 2 seems more chemically likely). The remaining ligand atoms are likely oxygen (more than three nitrogen ligands and sulfur ligation can be excluded), although the precise chemical species are unknown. Where [CEL + CS + CuONPs] and [CEL + KER + CuONPs] differ significantly is that [CEL + CS + CuONPs] exhibits a dependence of the EPR spectrum on the orientation of films of the material in the scanned magnetic field. In the perpendicular] | [orientation, there are significant projections of both the $g_{||}$ direction and the $g_{\perp}$ plane along the magnetic field, i.e., perpendicular to the film itself. Conversely, in the]–[orientation, there is only a small projection of the $g_{||}$ direction along the magnetic field, whereas there is a large projection of the $g_{\perp}$ plane along the field, i.e., in the plane of the film.

The EPR spectra of [CEL + CS + CuONPs] and [CEL + KER + CuONPs] exhibit $g_{||} > g_{\perp}$ and $A_{||} \sim 190 \times 10^{-4}$ cm^{-1}. These features indicate square-planar-based geometry, in which the paramagnetic electron nominally resides in the d$x^2 - y^2$ orbital perpendicular to the equatorial coordination plane, although lowering of ideal symmetry results in mixing-in of the dxy orbital.[32-37] Therefore, the contribution of the $g_{\perp}$ Zeeman manifold to the spectra of [CEL + CS + CuONPs] in all orientations indicates that the Cu(II) equatorial coordination plane is nominally parallel to, but substantially tilted with respect to, the plane of the film. The lack of any x–y orientation dependence in the plane of the film of the EPR spectra and the low values of |ΔO.P.| of 1.5–2.0 compared to ∼14 for a completely ordered system (Figures SI-4 and SI-5) indicate that the tilted planes are attached by sides that are randomly oriented in the plane of the film and that, therefore, the axial paramagnetic d$x^2 - y^2$ orbitals of the ensemble of Cu(II) ions describe a cone whose axis is

perpendicular to the film. Each of the individual d$x^2 - y^2$ orbitals will contribute equally, and in proportion to the sine of the half-angle of the cone, to the intensity of the $g_{||}$ resonance in the spectrum with the film in the] | [orientation. However, the contribution of each to the intensity of the $g_{||}$ resonance in the spectrum with the film in the]–[orientation will be proportional to the product of the sine of the half-angle of the cone and the cosine of the angle between the projection of the orbital on the film and the direction of the field. The proposed geometry, presented graphically as Figure SI-6, explains well the orientation dependence of the EPR spectra (see also the text in Supporting Information).

Property of the [CEL + CS/KER + CuONPs] Composites

Antimicrobial Activity of CuONPs is Dose-Dependent

We have previously shown that [CEL + CS] composites inhibit growth of various bacteria, including *E. coli* and *S. aureus.*[15-21] To determine if adding CuO nanoparticles into the composite could enhance and/or extend its antibacterial activity, cultures in logarithmic-phase growth were subcultured into fresh broth and incubated for 16 h in the presence of [CEL + CS + CuONPs] composite and [CEL + CS] control composite. As shown in Figure 6, compared to the control, growth of a wide range of microorganisms, including highly resistant *E. coli*, MRSA ATCC 33591, *S. agalactiae*, *E. cloacae*, *P. aeruginosa* ATCC 27853, VRE, *E. coli* ATCC 25922, and *S. maltophilia*, was reduced in the presence of [CEL + CS + CuONPs] composite. As expected, for all bacteria, the antibacterial activity was found to be correlated with the content of CuONPs in the composites. With the exception of MRSA ATCC 33591, *P. aeruginosa* ATCC 27853, and *S. maltophilia*, observed reductions of growth were between 1.90 and 4.69 $\log_{10}$ higher in the presence of [CEL + CS + 298 nmol/mg CuONPs] (Figure 6, yellow bars) compared to [CEL + CS + 35 nmol/mg CuONPs] (red bars). Incubation of MRSA ATCC 33591 and *S. maltophilia* in the presence of [CEL + CS + 434 nmol/mg CuONPs] (green bars) resulted in additional 3.08 and 1.61 $\log_{10}$ reductions in growth, respectively, compared to [CEL + CS + 298 nmol/mg CuONPs] (yellow bars). In limited experimentation, [CEL + CS + 596 nmol/mg CuONPs] (blue bars) caused significant reduction in growth of highly resistant *E. coli*, *P. aeruginosa* ATCC 27853, and *E. coli* ATCC 25992 (Figure 7). It is of particular interest to note that even with only 37.7 µmol CuO concentration, the [CEL + CS + 35 nmol/mg CuONPs] composite still exhibits substantial growth reduction for all bacteria tested.

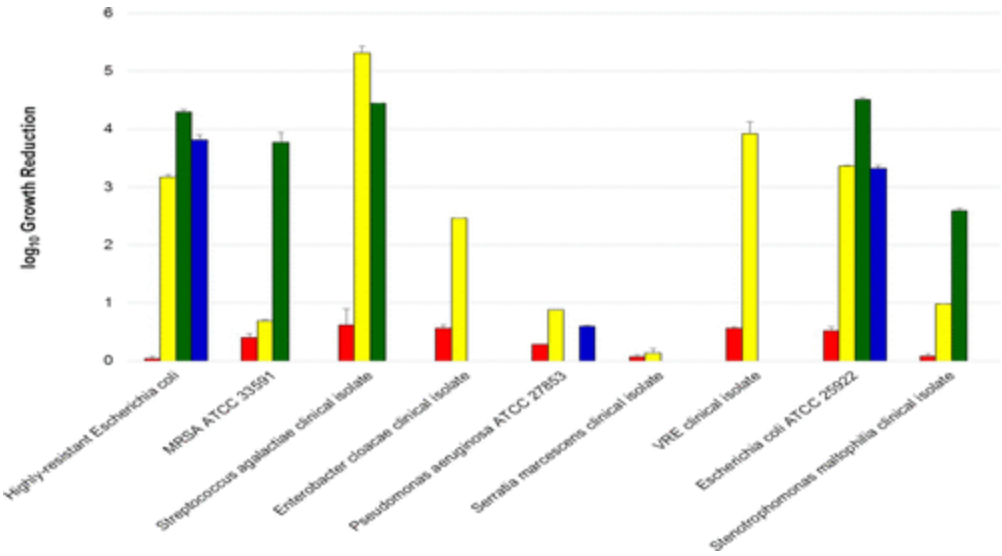

Figure 6. Growth reduction of characterized and clinical bacterial isolates following treatment with [CEL + CS + CuONPS] relative to growth in [CEL + CS]. Red bars: [CEL + CS + 35 nmol/mg CuONPs]; yellow bars: [CEL + CS + 298 nmol/mg CuONPs]; green bars: [CEL + CS + 434 nmol/mg CuONPs]; blue bars: [CEL + CS + 596 nmol/mg CuONPs].

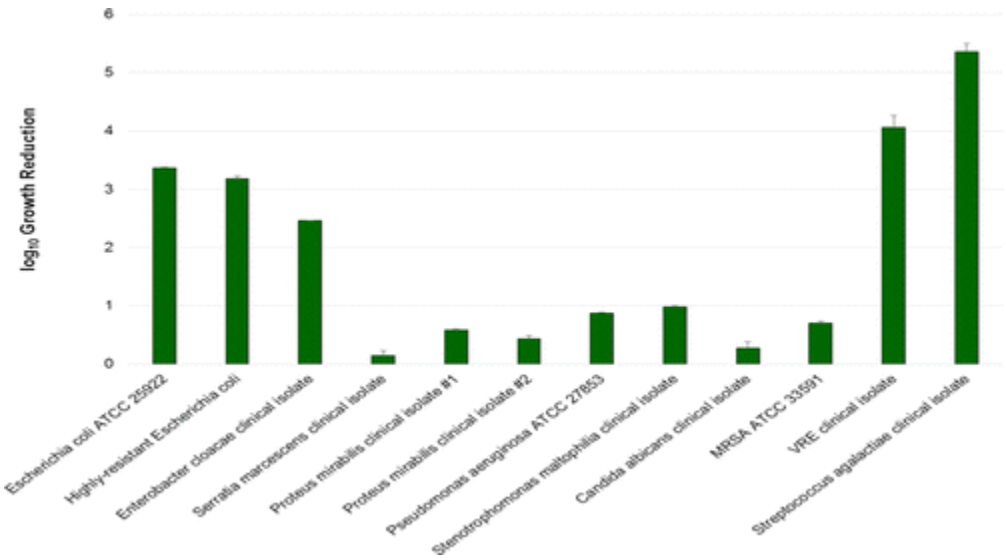

Figure 7. Growth reduction of characterized and clinical bacterial isolates following treatment with [CEL + CS + 298 nmol/mg CuONPS] relative to growth in [CEL + CS].

Currently, the exact mechanism of antimicrobial activity of copper oxide is not known. It was proposed by many investigators that reactive oxygen species produced through Fenton-type reactions leading to DNA damage is the main mechanism for its antibacterial activity.[(40-44)] Regarding the role of different species of CuONPs on the antibacterial activity, considering the fact

that the monomeric species, whose unique spatial orientation is only 25% of the total CuO, with the remaining 75% due to aggregated large nanoparticles. At higher levels of added copper oxide (>59 nmol/mg), the additional copper was mainly the latter species, i.e., the EPR-silent aggregated large nanoparticles. This together with the fact that the antibacterial activity of the composites correlates with the concentration of CuONPs seems to indicate that the antibacterial activity is probably due to the aggregated, large nanoparticle species. However, more study is needed to fully understand the antibacterial property of the CuONP composites.

Selectivity of Antimicrobial Activity

The antimicrobial effect of [CEL + CS + CuONPs] composites appeared to be selective. Clinical isolates of *C. albicans* and *Serratia marcescens* demonstrated marginal growth reduction (0.15–0.27 $\log_{10}$) in the presence of [CEL + CS + 310 μmol CuONPs] compared to [CEL + CS] control (Figure 7). Nonglucose-fermentative Gram-negative bacillus isolates *P. aeruginosa* ATCC 27853 and *S. maltophilia* both exhibited an approximate 1 $\log_{10}$ growth reduction in the presence of [CEL + CS + 298 nmol/mg CuONPs]. It is also evident from Figure 7 that [CEL + CS + CuONPs] exhibits significant reduction in growth of both Gram-negative enteric (*E. coli* ATCC 25922, highly resistant *E. coli*, *E. cloacae*) and Gram-positive (VRE, *S. agalactiae*) organisms. Two clinical isolates of *P. mirabilis* showed similar $\log_{10}$ growth reduction values (0.44 and 0.59) in the presence of [CE + CS + 298 nmol/mg CuONPs].

Biocompatibility of [CEL + CS + CuONPs]

We have previously shown that [CEL + CS] has no deleterious effect on the proliferation and viability of eukaryotic cells. To determine the effect of [CEL + CS + CuONPs] on human fibroblasts, in vitro cultures were subjected to the composite for 3 days prior to morphologic and proliferation assessment. As shown in Figure 8, fibroblast cultures that were treated with [CEL + CS + 596 nmol/mg CuONPs] generated 108.8% less metabolic activity than fibroblasts incubated with [CEL + CS] (Figure 8) and exhibited a rounded, noncontiguous monolayer distribution in contrast to control cultures (Figure 9A,B). Similar effects were observed with [CEL + CS + 298 nmol/mg CuONPs] (Figures 8 and 9C,D). Furthermore, treatment of cultures with [CEL + CS + 59 nmol/mg CuONPs] and [CEL + CS + 108 nmol/mg CuONPs] resulted in fibroblast metabolic activities that represented (34 ± 8) and (53 ± 8)% of the activity from cultures treated with [CEL + CS] (Figure 8). Decreased monolayer density and preliminary changes in fibroblast morphology were noted in these cultures (Figure 9F,H) compared to tandem fibroblast cultures treated with [CEL + CS] (Figure 9E,G). Of particular interest, the metabolic activity of fibroblasts incubated with [CEL + CS + 35 nmol/mg CuONPs] was at (94 ± 3)% of the level of control-treated fibroblasts (Figure 8). As expected, no observable changes in fibroblast morphology were detected between [CEL + CS]-treated cultures (Figure 9I) and cultures treated with [CEL + CS + 35 nmol/mg CuONPs] (Figure 9J). As specified in ISO 10993-5: 2009(E), a material is not cytotoxic if the viability of fibroblasts after the exposure is greater than 70% of control activity.[45] The data presented suggest that [CEL + KER + CuONPs] is toxic to human fibroblasts if it contains high concentration of CuONPs (i.e., 35 nmol/mg of composite). However, at or below CuO concentration of 37.7 μmol, the [CEL + CS + CuONPs] composite is not only biocompatible, but also retains antimicrobial activity against a wide range of microorganisms, including highly resistant *E. coli*, MRSA ATCC 33591, *S. agalactiae*, *E. cloacae*, *P. aeruginosa* ATCC 27853, VRE, *E. coli* ATCC 25922, *S. maltophilia*, *S. marcescens*, and *C. albicans*.

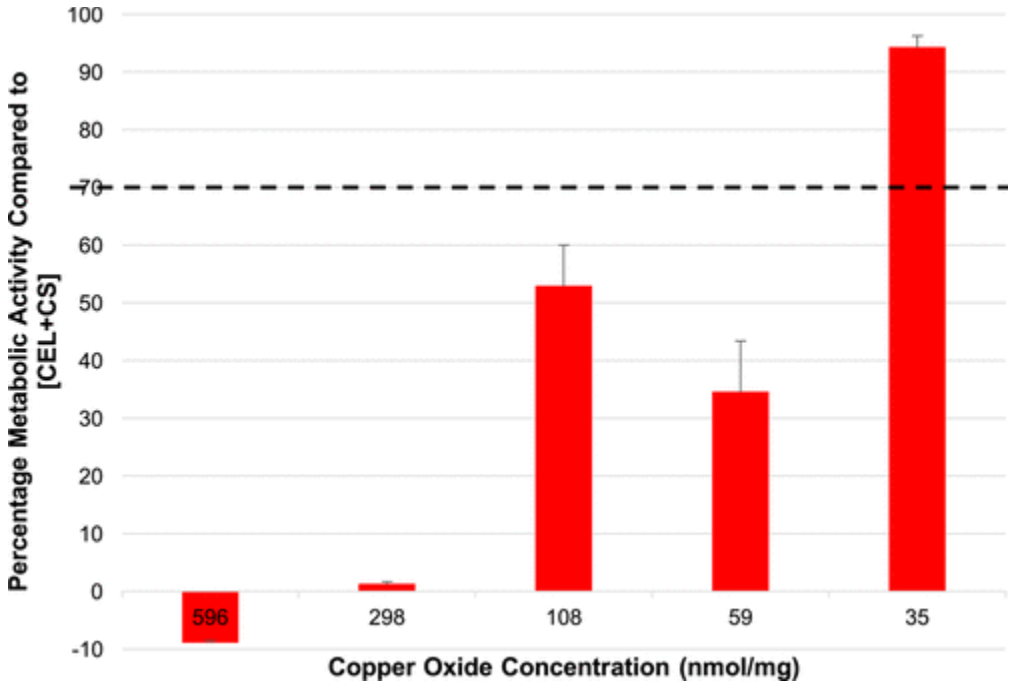

Figure 8. Relative metabolic activity of ATCC CRL-2522 fibroblasts, as determined by nonradiometric cell proliferation assays, following treatment with [CEL + CS + CuONPs].

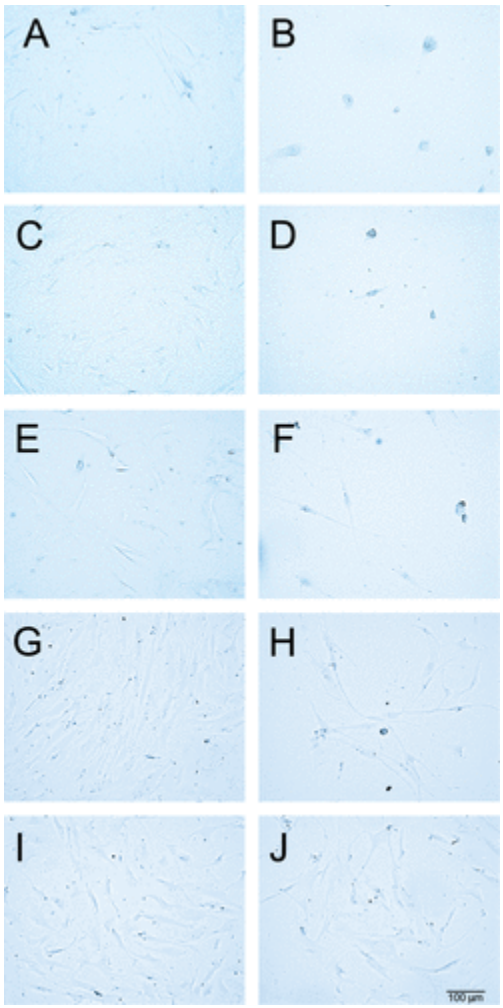

Figure 9. Photomicrographs of ATCC CRL-2522 monolayers following incubation with [CEL + CS] composite (A, C, E, G. I) and following tandem incubation with [CEL + CS] composite containing 596 nmol/mg (B), 298 nmol/mg (D), 108 nmol/mg (F) 59 nmol/mg (H), and 35 nmol/mg (J) CuONPs.

Conclusions

In summary, we have shown that biocompatible composites containing copper oxide nanoparticles (CuONPs) were successfully synthesized from abundant and sustainable polysaccharides and protein (CEL, CS, and KER) in a green and facile method, in which [$BMIm^+Cl^-$], a simple ionic liquid, was used as the sole solvent. FTIR, SEM, EDS, and X-ray diffraction results indicate that CEL, CS, and KER remained chemically intact and were homogeneously distributed in the composites with CuONPs of 22 ± 1 nm. Microbial assays indicate that the [CEL + CS + CuONPs] composites exhibited bactericidal activity against a wide range of bacteria and fungi, including highly resistant *E. coli*, MRSA ATCC 33591, *S. agalactiae*, *E. cloacae*, *P. aeruginosa* ATCC 27853, VRE, *E. coli* ATCC 25922, and *S. maltophilia*. As expected, for all bacteria, the antibacterial activity was found to be correlated with the content of CuONPs in the composites. For example, in the presence of the [CEL + CS + 298 nmol/mg CuONPs] composite, observed reductions of bacterial growth were between 1.90 and 4.69 $\log_{10}$ higher compared to [CEL + CS + 35 nmol CuONPs]. The

antimicrobial effect of the [CEL + CS + CuONPs] composites appeared to be selective. More importantly, at a [CuONPs] concentration of 35 nmol/mg or lower, the bactericidal activity of the composite was complemented by its biocompatibility with human fibroblasts. Electron microscopy indicates a fibrous structure for [CEL + CS]. EPR data identify two species that likely preclude the formation of fully developed nanoparticles: (1) a well-characterized tetragonal monomeric species and (2) a broad and unresolved species. In [CEL + CS + CuONPs], but not [CEL + KER + CuNPs], the CS-bound monomeric copper is uniquely oriented relative to the plane of the [CEL + CS + Cu] composite films. In both films, the Cu(II) is bound via equatorial nitrogen ligand atoms (likely two), and probably with additional oxygen ligand atoms. This provides information on the initial binding of Cu(II) to the composite substrate and explains the strong attachment of the nanoparticles to the substrate. The second, broad, paramagnetic species is not dissimilar to CuO and is likely due to nascent protonanoparticles and/or Cu(II) ions on the surface of mature nanoparticles. Taken together, the results presented clearly show that the [CEL + CS + CuONPs] composites are biocompatible and possess excellent bactericidal activity against pathogenic bacteria and fungi, including bacteria that are highly resistant to antibiotics. The [CEL + CS + CuONPs] composites thus have all required property for use as high-performance materials for a wide range of applications, including dressing to treat chronic ulcerous infected wounds. These are subject of our current intense investigation.

Supporting Information

Supporting Information for Biocompatible Copper Oxide Nanoparticle Composites from Cellulose and Chitosan: Facile Synthesis, Unique Structure and Antimicrobial Activity

Chieu D. Tran
Department of Chemistry, Marquette University, Milwaukee, WI
James Makuvaza
Department of Chemistry, Marquette University, Milwaukee, WI
Erik Munson
Department of Chemistry, Marquette University, Milwaukee, WI
Brian Bennett
Department of Physics, Marquette University, Milwaukee, WI

Corresponding author: Tel. (414) 288 5428; email: chieu.tran@marquette.edu

Additional consideration of the geometry of Cu(II) bound to [CEL+CS+CuONPs]

There is one alternative explanation that is geometrically appealing but is inconsistent with the observed value for A||. If Cu(II) were bound to the film by two nitrogen atoms forming one side of the base of a square pyramid, with the base protruding perpendicularly to the film, then the g|| and

gx directions would project along the Cu-N bonds pointing diagonally out of the plane and the axial direction would now correspond to gy, lying parallel to the plane.39 This scenario would equally well explain the orientation-dependence of the EPR spectra. However, the necessity of adopting square pyramidal geometryin order to accommodate the reorientation of the g-tensor would also require a much smaller value (~130 - 140 G) for A|| than is observed here. Figure S6, then, appears to represent the only structural model that is consistent with all the data.

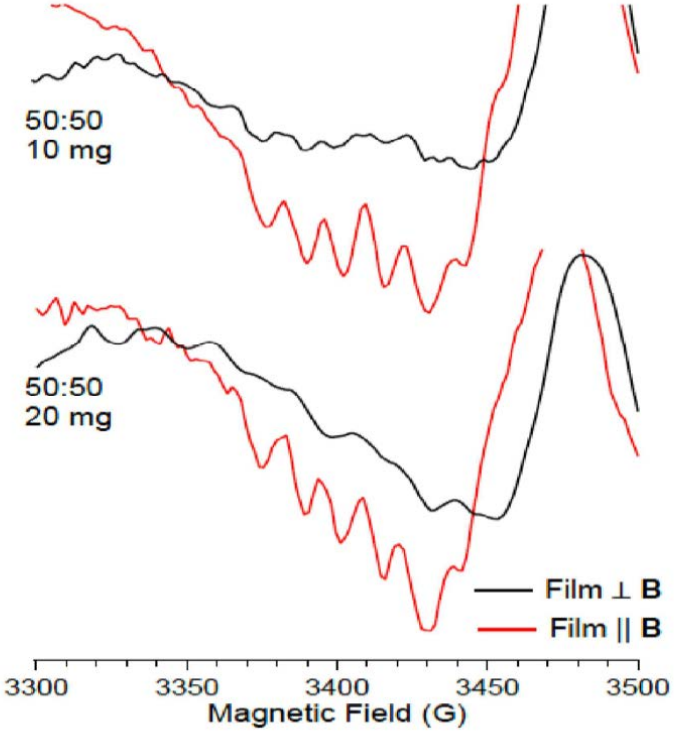

Figure SI-1. Orientation-dependent hyperfine structure in the g⊠ region of the EPR spectrum of [CEL+CS+CuONPs] composites. The spectra are of 50:50 [CEL+CS] composites with 10 mg and 20 mg CuONPs, oriented both parallel and perpendicular to the scanned magnetic field.

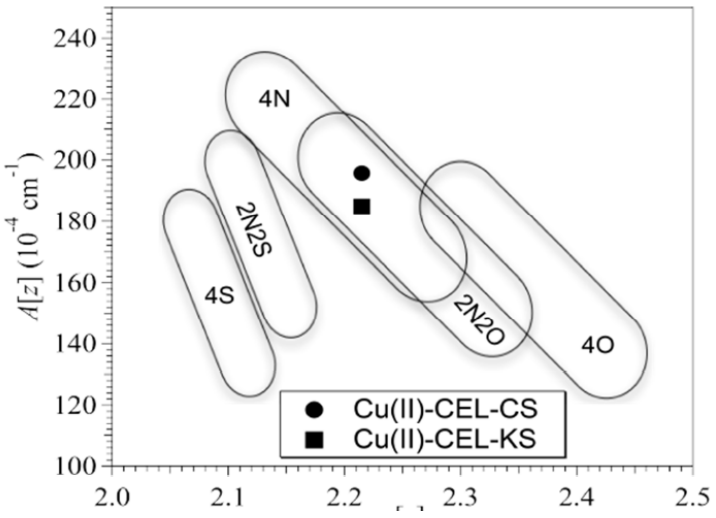

Figure SI-2. Peisach-Blumberg analysis of the gII regions of the spectra of [CEL+CS+CuNPs] and [CEL+KE+CuNPs]. For both 50:50 CEL-CS and 50:50 CEL-KE, the plot indicates that the tetragonal Cu(II) ion responsible for the 63/65Cu-hyperfine-exhibiting EPR signal is equatorially-coordinated by at least two nitrogen atoms.

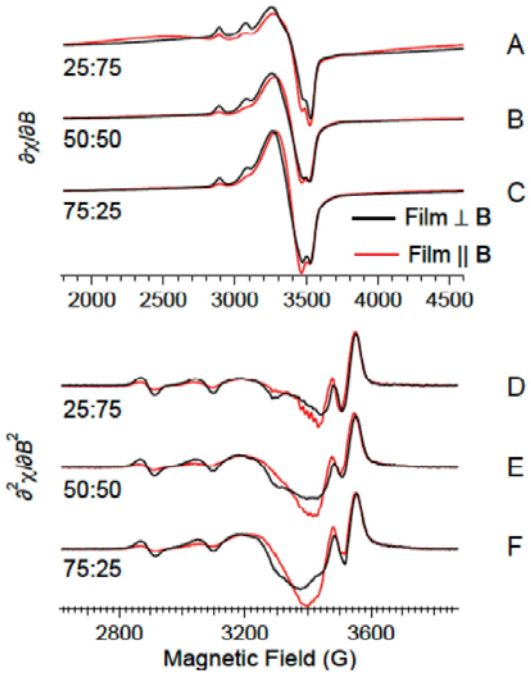

Figure SI-3. Selected EPR spectra of Cu(II) in [CEL+CS+CuNPs] composites as a function of the CEL and CS compositions. Spectra are shownwith films oriented both parallel and perpendicular to the scanned magnetic field, in the first and second derivative displays. Intensities have been normalized. Traces A-C correspond to substrates of CEL:CS in proportions 25:75, 50:50, and 75:25, respectively. Traces D-F are pseudomodulations of the spectra of traces A-C generated using a pseudomodulation amplitude of 4 G (0.4 mT).

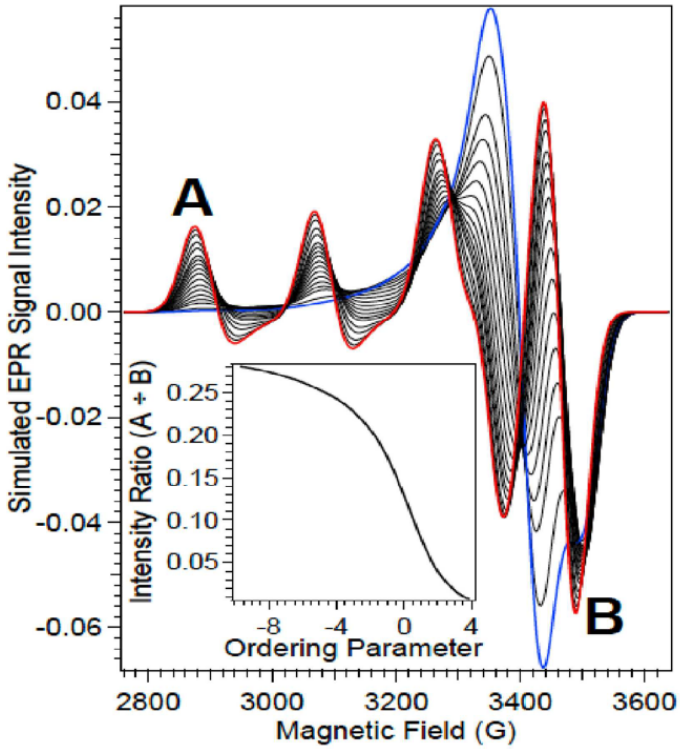

Figure SI-4. Construction of a calibration curve relating an orientationally ordering parameter to an experimentally accessible parameter. Computer simulations were carried out including an ordering parameter that effectively calculates the spectrum with a range of orientation specificities, from a large negative parameter (gII parallel ot B; indicated by the red trace), through zero (no orientation, i.e. a poweder spectrum), to a large positive (gII perpendicular to B; indicated by the blue trace). The ratios of the intensities of the features labelled “A” and “B” in the main figure were then plotted against the ordering parameter to construct the calibration curve shown in the inset.

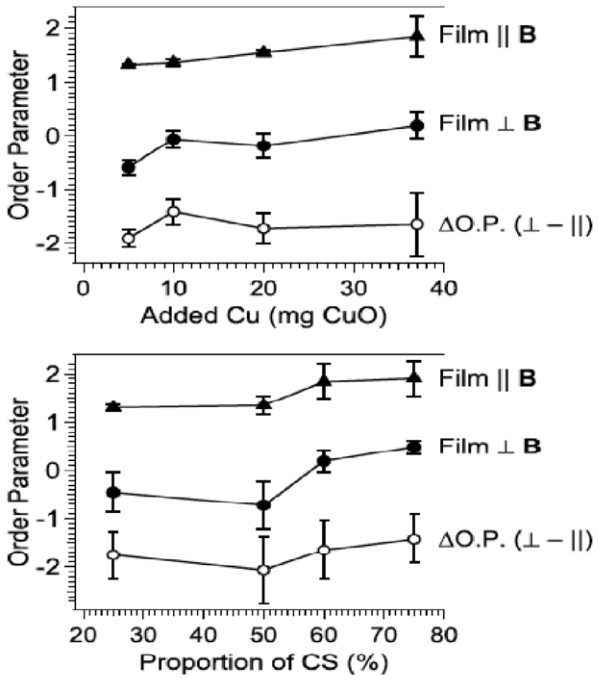

Figure SI-5. Order parameters for [CEL+CS+CuNPs]. Ordering parameters for various [CEL+CS+CuNPs] formulations are shown, calculated from the ratios of the lowest and highest field line intensities and the correlation curve of Figure 7, for films oriented both parallel and perpendicular to the scanned magnetic field. The magnitude of the difference between the ordering parameters at the two orientations is an indicator of the extent of orientation of the Cu(II) by the film and the difference is plotted as "⊠ O.P." for each formulation.

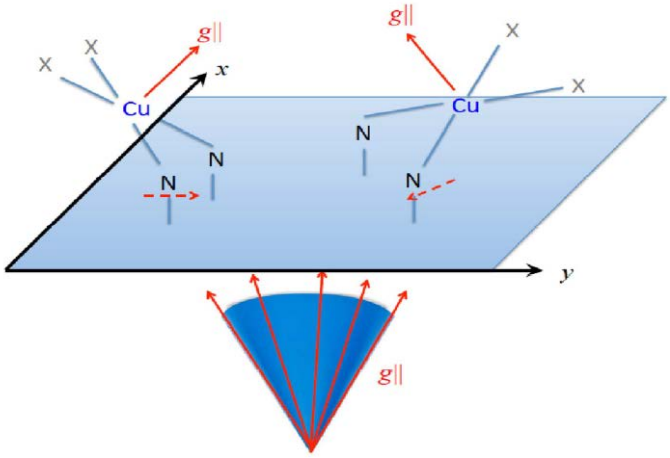

Figure SI-6. Proposed geometry of Cu in [CEL+CS+CuONPs] composite. The ligand labeled X is likely oxygen, from chemical consideration, but is not unambiguously identifiable as such by EPR spectroscopy.

The authors declare no competing financial interest.

Acknowledgment

EPR spectroscopy was supported by a Major Research Instrumentation Award (NSF CHE-1532168 to B.B. and Richard C. Holz), Bruker Biospin, Marquette University, and the Todd Wehr Foundation (to B.B.). The authors thank Daniel Holbus at Marquette University for skilled fabrication of the sample mounting apparatus.

References

1 Borkow, G. Using Copper to Improve the Well-Being of the Skin Curr. Chem. Biol. 2015, 8, 89–102 DOI: 10.2174/2212796809666150227223857

2 Monk, A. B.; Kanmukhla, V.; Trinder, K.; Borkow, G. Potent Bactericidal Efficacy of Copper Oxide Impregnated Non-Porous Solid Surfaces BMC Microbiol. 2014, 14, 57 DOI: 10.1186/1471-2180-14-57

3 Imai, K.; Ogawa, H.; Bui, V. N.; Inoue, H.; Fukuda, J.; Ohba, M.; Yamamoto, Y.; Nakamura, K. Inactivation of High and Low Pathogenic Avian Influenza Virus H5 Subtypes by Copper Ions Incorporated in Zeolite-Textile Materials Antiviral Res. 2012, 93, 225– 233 DOI: 10.1016/j.antiviral.2011.11.017

4 Lazary, A.; Weinberg, I.; Vatine, J.-J.; Jefidoff, A.; Bardenstein, R.; Borkow, G.; Ohana, N. Reduction of Healthcare-associated Infections in a Long-term Care Brain Injury Ward by Replacing Regular Linens with Biocidal Copper Oxide Impregnated Linens Int. J. Infect. Dis. 2014, 24, 23– 29 DOI: 10.1016/j.ijid.2014.01.022

5 Fujimori, Y.; Sato, T.; Hayata, T.; Nagao, T.; Nakayama, M.; Nakayama, T.; Sugamata, R.; Suzuki, K. Novel Antiviral Characteristics of Nanosized Copper(I) Iodide Particles Showing Inactivation Activity Against 2009 Pandemic H1N1 Influenza Virus Appl. Environ. Microbiol. 2011, 120, 951– 955 DOI: 10.1128/aem.06284-11

6 Eser, O. K.; Ergin, A.; Hascelik, G. Antimicrobial Activity of Copper Alloys Against Invasive Multidrug-resistant Nosocomial Pathogens Curr. Microbiol. 2015, 71, 291– 295 DOI: 10.1007/s00284-015-0840-8

7 Zhang, Q.; Zhang, K.; Xu, D.; Yang, G.; Huang, H.; Nie, F.; Liu, C.; Yang, S. CuO Nanostructures: Synthesis, Characterization Growth Mechanisms, Fundamental Properties, and Applications Prog. Mater. Sci. 2014, 60, 208– 337 DOI: 10.1016/j.pmatsci.2013.09.003

8 Sankar, R.; Baskaran, A.; Shivashangari, K. S.; Ravikumar, V. Inhibition of Pathogenic Bacterial Growth on Excision Wound by Green Synthesized Copper Oxide Nanoparticles Leads to Accelerated Wound Healing Activity in Wistar Albino Rats J. Mater. Sci.: Mater. Med. 2015, 26, 214– 231 DOI: 10.1007/s10856-015-5543-y

9 Yang, X.; Yang, M.; Pang, B.; Vara, M.; Xia, Y. Gold Nanomaterials at Work in Biomedicine Chem. Rev. 2015, 115, 10410– 10488 DOI: 10.1021/acs.chemrev.5b00193

10 Mitragotri, S. Accelerating the Translation of Nanomaterials in Biomedicine ACS Nano 2015, 9, 6644– 6654 DOI: 10.1021/acsnano.5b03569

11 Xia, X.; Zeng, J.; Zhang, Q.; Moran, C. H.; Xia, Y. Recent Developments in Shape-Controlled Synthesis of Silver Nanocrystals J. Phys. Chem. C 2012, 116, 21647– 21656 DOI: 10.1021/jp306063p

12 Hammond, P. T.; Hersam, M. C.; Javey, A.; Kotov, N. A.; Weiss, P. S. A Year for Nanoscience ACS Nano 2014, 8, 11901– 11903 DOI: 10.1021/nn5070716

13 Pelaz, B.; Kotov, N. A.; Liz-Marzán, L. M. The State of Nanoparticle-based Nanoscience and Biotechnology: Progress, Promises, and Challenges ACS Nano 2012, 6, 8468– 8483 DOI: 10.1021/nn303929a

14 Shahmiri, M.; Ibrahim, N. A.; Shayesteh, F.; Asim, N.; Motallebi, N. Preparation of PVP-coated Copper Oxide Nanosheets as Antibacterial and Antifungal Agents J. Mater. Res. 2013, 28, 3109– 3118 DOI: 10.1557/jmr.2013.316

15 Duri, S.; Tran, C. D. Supramolecular Composite Materials from Cellulose, Chitosan, and Cyclodextrin: Facile Preparation and their Selective Inclusion Complex Formation with Endocrine Disruptors Langmuir 2013, 29, 5037– 5049 DOI: 10.1021/la3050016

16 Tran, C. D.; Duri, S.; Delneri, A.; Franko, M. Chitosan–cellulose Composite Materials: Preparation, Characterization and Application for Removal of Microcystin J. Harard. Mater. 2013, 252–253, 355– 366 DOI: 10.1016/j.jhazmat.2013.02.046

17 Tran, C. D.; Mututuvari, T. M. Cellulose, Chitosan and Keratin Composite Materials. Controlled Drug Release Langmuir 2015, 31, 1516– 1526 DOI: 10.1021/la5034367

18 Tran, C. D.; Mututuvari, T. M. Cellulose, Chitosan and Keratin Composite Materials. Facile and Recyclable Synthesis, Conformation and Properties ACS Sustainable Chem. Eng. 2016, 4, 1850– 1861 DOI: 10.1021/acssuschemeng.6b00084

19 Tran, C. D.; Prosenc, F.; Franko, M.; Benzi, G. Green Composites from Cellulose, Wool, Hair and Chicken Feather. Synthesis, Structure and Antimicrobial Property Carbohydr. Polym. 2016, 151, 1269– 1276 DOI: 10.1016/j.carbpol.2016.06.021

20 Xie, H.; Li, S.; Zhang, S. Ionic liquids as Novel Solvents for the Dissolution and Blending of Wool Keratin Fibers Green Chem. 2005, 7, 606– 608 DOI: 10.1039/b502547h

21 Zhu, S.; Wu, Y.; Chen, Q.; Yu, Z.; Wang, C.; Jin, S.; Ding, Y.; Wu, G. Dissolution of Cellulose with Ionic Liquids and its Application: A Mini-review Green Chem. 2006, 8, 325– 327 DOI: 10.1039/b601395c

22 Mututuvari, T. M.; Harkins, A. L.; Tran, C. D. Facile Synthesis, Characterization and Antimicrobial Activity of Cellulose–chitosan–hydroxyapatite Composite Material: A Potential Material for Bone Tissue Engineering J. Biomed. Mater. Res., Part A 2013, 101, 3266–3277 DOI: 10.1002/jbm.a.34636

23 Stoll, S.; Schweiger, A. EasySpin, a Comprehensive Software Package for Spectral Simulation and Analysis in EPR J. Magn. Reson. 2006, 178, 42– 55 DOI: 10.1016/j.jmr.2005.08.013

24 Ovchinnikov, I. V.; Konstaninov, V. N. Extra Absorption Peaks in EPR Spectra of Systems with Anisotropic *g*-Tensor and Hyperfine Structure in Powders and Glasses J. Magn. Reson. 1978, 32, 179– 190 DOI: 10.1016/0022-2364(78)90203-2

25 Przepiórski, J.; Morawski, A. W.; Oya, A. Method for Preparation of Copper-coated Carbon Material Chem. Mater. 2003, 15, 862– 865 DOI: 10.1021/cm021220+

26 Haber, J.; Machej, T.; Ungier, L.; Ziółkowski, J. ESCA Studies of Copper Oxides and Copper Molybdates J. Solid State Chem. 1978, 25, 207– 218 DOI: 10.1016/0022-4596(78)90105-6

27 Guo, Z.; Fang, J.; Wang, L.; Liu, W. Fabrication of Superhydrophobic Copper by Wet Chemical Reaction Thin Solid Films 2007, 515, 7190– 7194 DOI: 10.1016/j.tsf.2007.02.100

28 Lamprecht, E.; Watkins, G. M.; Brown, M. E. The Thermal Decomposition of Copper(II) Oxalate Revisited Thermochim. Acta 2006, 446, 91– 100 DOI: 10.1016/j.tca.2006.03.008

29 Scherrer, P. Bestimmung der Grösse und der Inneren Struktur von Kolloidteilchen Mittels Röntgenstrahlen Nachr. Ges. Wiss. Göttingen, Math.–Phys. Kl. 1918, 26, 98– 100

30 Langford, J. I.; Wilson, A. J. C. Scherrer after Sixty Years: A Survey and Some New Results in the Determination of Crystallite Size J. Appl. Crystallogr. 1978, 11, 102– 113 DOI: 10.1107/S0021889878012844

31 Kowalski, J. M.; Bennett, B. Spin Hamiltonian Parameters for Cu(II)–Prion Peptide Complexes from L-Band Electron Paramagnetic Resonance Spectroscopy J. Am. Chem. Soc. 2011, 133, 1814– 1823 DOI: 10.1021/ja106550u

32 Maki, A. H.; McGarvey, B. R. Electron Spin Resonance in Transition Metal Chelates. I. Copper(II) Bis-Acetylacetonate J. Chem. Phys. 1958, 29, 31– 34 DOI: 10.1063/1.1744456

33 Maki, A. H.; McGarvey, B. R. Electron Spin Resonance in Transition Metal Chelates. II. Copper(II) Bis-Salicylaldehyde-Imine J. Chem. Phys. 1958, 29, 35– 38 DOI: 10.1063/1.1744457

34 Pilbrow, J. R. Transition Ion Electron Paramagnetic Resonance; Oxford University Press: Oxford, 1990.

35 Solomon, E. I.; Heppner, D. E.; Johnston, E. M.; Ginsbach, J. W.; Cirera, J.; Qayyum, M.; Kieber-Emmons, M. T.; Kjaergaard, C. H.; Hadt, R. G.; Tian, L. Copper Active Sites in Biology Chem. Rev. 2014, 114, 3659– 3853 DOI: 10.1021/cr400327t

36 Antholine, W. E.; Bennett, B.; Hanson, G. R. Copper Coordination Environments. In Multifrequancy Electron Paramagnetic Resonance; Misra, S. K., Ed.; Wiley-VCH: Berlin, 2011.

37 Bennett, B.; Kowalski, J. M. EPR Methods for Biological Cu(II): L-Band CW and NARS Methods Enzymol. 2015, 563, 341– 361 DOI: 10.1016/bs.mie.2015.06.030

38 Peisach, J.; Blumberg, W. E. Structural Implications Derived from the Analysis of Electron Paramagnetic Resonance Spectra of Natural and Artificial Copper Proteins Arch. Biochem. Biophys. 1974, 165, 691– 708 DOI: 10.1016/0003-9861(74)90298-7

39 Chikira, M.; Tomizawa, Y.; Fukita, D.; Sugizaka, T.; Sugawara, N.; Yamazaki, T.; Sasano, A.; Shindo, H.; Palaniandavar, M.; Antholine, W. E. DNA-fiber EPR Study of the Orientation of Cu(II) Complexes of 1,10-phenanthroline and its Derivatives Bound to DNA: Mono(phenanthroline)-copper(II) and its Ternary Complexes with Amino Acids J. Inorg. Biochem. 2002, 89, 163– 173 DOI: 10.1016/S0162-0134(02)00378-1

40 Wang, X.; Li, J.; Liu, R.; Hai, R.; Zou, D.; Zhu, X.; Luo, N. Responses of Bacterial Communities to CuO Nanoparticles in Activated Sludge System Environ. Sci. Technol. 2017, 51, 5368–5376 DOI: 10.1021/acs.est.6b06137

41 Karlsson, H. L.; Cronholm, P.; Gustafsson, J.; Möller, L. Copper Oxide Nanoparticles are Highly Toxic: A Comparison Between Metal Oxide Nanoparticles and Carbon Nanotubes Chem. Res. Toxicol. 2008, 21, 1726– 1732 DOI: 10.1021/tx800064j

42 Nel, A.; Xia, T.; Mädler, L.; Li, N. Toxic Potential of Materials at the Nanolevel Science 2006, 311, 622– 627 DOI: 10.1126/science.1114397

43 Hassan, I. A.; Parkin, I. P.; Nair, S. P.; Carmalt, C. J. Antimicrobial Activity of Copper and Copper Oxide Thin Films Deposited via Aerosol-assisted CVD J. Mater. Chem. B 2014, 2, 2855– 2960 DOI: 10.1039/C4TB00196F

44 Grass, G.; Rensing, C.; Solioz, M. Metallic Copper as an Antimicrobial Surface Appl. Environ. Microbiol. 2011, 77, 1541– 1547 DOI: 10.1128/AEM.02766-10

45 ISO 10993. Biological Evaluation of Medical Devices – Part 5: Tests for in Vitro Cytotoxicity; The International Organization for Standardization: Geneva, Switzerland, 2009. www.iso.org/obp/ui/#iso:std:iso:10993:-5:ed-3:v1:en.